Fine Structure and Physical Properties of Polyethylene/Poly(ethylene terephthalate) Bicomponent Fibers in High-Speed Spinning. I. Polyethylene Sheath/Poly(ethylene terephthalate) Core Fibers

H. H. CHO,[1] K. H. KIM,[1] Y. A. KANG,[1] H. ITO,[2] T. KIKUTANI[2]

[1] Department of Textile Engineering, Pusan National University, Pusan 609-735, Korea

[2] Department of Organic and Polymeric Materials, Tokyo Institute of Technology, 2-12-1, O-Okayama, Meguro-Ku, Tokyo 152, Japan

Received 7 September 1999; accepted 1 December 1999

ABSTRACT: The high-speed melt spinning of sheath/core type bicomponent fibers was performed and the change of fiber structure with increasing take-up velocity was investigated. Two kinds of polyethylene, high density and linear low density (HDPE, LLDPE) with melt flow rates (MFR) of 11 and 50, [HDPE(11), LLDPE(50)], and poly(ethylene terephthalate) (PET) were selected and two sets of sheath/core combinations [HDPE(11)/PET and LLDPE(50)/PET bicomponent fibers] were studied. The fiber structure formation and physical property effects on the take-up velocities were investigated with birefringence, wide-angle X-ray diffraction, thermal analysis, tensile tests, and so forth. In the fiber structure formation of PE/PET, the PET component was developed but the PE components were suppressed in high-speed spinning. The different kinds of PE had little affect on the fine structure formation of bicomponent fibers. The difference in the mechanical properties of the bicomponent fiber with the MFR was very small. The instability of the interface was shown above a take-up velocity of 4 km/min, where the orientation-induced crystallization of PET started. LLDPE(50)/PET has a larger difference in intrinsic viscosity and a higher stability of the interface compared to the HDPE(11)/PET bicomponent fibers. © 2000 John Wiley & Sons, Inc. J Appl Polym Sci 77: 2254–2266, 2000

Key words: polyethylene; poly(ethylene terephthalate); melt spinning; fine structure; physical properties

INTRODUCTION

The bicomponent melt-spinning process is one in which two polymers are coextruded to form a single filament with a designed cross-sectional arrangement, and it has received considerable commercial interest because of its potential applications in the production of various specialty fibers such as crimped fibers, thermal bonding fibers, electrical conductive fibers, ultrafine fibers, and noncircular cross-sectional fibers.[1–4]

Among these, thermal bonding of sheath/core type bicomponent fiber is used in nonwoven fabrics. This bicomponent fiber for nonwoven fabrics is used with a difference in the melting temperatures: that is, one polymer has a lower melting temperature in the sheath and the other polymer has a higher melting temperature in the core.

Correspondence to: H. H. Cho.

Journal of Applied Polymer Science, Vol. 77, 2254–2266 (2000)

On the other hand, high-speed melt spinning can be obtained with filaments of low shrinkage and high tenacity. It is well known that a significant development of fiber structure occurs during high-speed spinning, and the structure and properties of as-spun fibers strongly depend on the thermal and stress histories of the molten polymer in the spinline.[5] When two polymers are coextruded in bicomponent spinning, the stress and thermal histories of each component are caused by the mutual interaction of two components, contrary to those in single-component spinning. Thus, by selecting a suitable combination of polymers, it might be possible to improve the structure of high-speed spun fibers.

Radhakrishnan et al.[6,7] used coextrusion to investigate for use on nonwoven fabrics the sheath/core type of bicomponent fiber from poly(ethylene terephthalate) (PET) polymers with high molecular weight PET (HMPET) as the sheath and low molecular weight PET (LMPET) as the core. The take-up velocity ranged from 1 to 7 km/min. The structures of the individual components in the as-spun bicomponent fibers were characterized. The orientation and orientation-induced crystallization of the HMPET component were enhanced while those of the LMPET component were suppressed in comparison to corresponding single-component spinning.

However, the LMPET/HMPET bicomponent fiber for nonwoven fabrics has stiffness and rigidity properties defects in the handling of the resulting nonwoven fabrics. Accordingly, the PE/PET bicomponent fiber may make up for the above defects in these nonwoven fabrics.

Kikutani et al.[8,9] reported the structure formation on high-speed melt spinning and the changes of fiber structure with increasing take-up velocity in polypropylene (PP)/PET and polystyrene (PS)/PET bicomponent fibers of sheath/core combinations. The development of molecular orientation and the start of orientation-induced crystallization of the PET component in PP/PET bicomponent fibers occurred at lower take-up velocities compared to single-component spinning. The PP component in the PP/PET showed low orientation of the pseudohexagonal structure in overall take-up velocities. On the contrary, the structure formation of PET in the PS/PET bicomponent fiber was suppressed and the molecular orientation of the PS component was enhanced.

Therefore, the fiber structure formation in the spinline depends on the component having a higher melt viscosity. The orientation of one component with the higher melt viscosity is better than that of the other component with the lower melt viscosity.

The high-speed spun PE/PET bicomponent fibers using two kinds of PE, which are high density PE (HDPE), linear low density PE (LLDPE), and PET polymers, were produced. Then the fiber structural formation in the spinline and the fine structure, physical properties, and interfacial morphology of as-spun fibers were investigated.

EXPERIMENTAL

High-Speed Spinning of Bicomponent Fiber

We produced sheath/core bicomponent fibers by extruding the melt of PE [melt flow rate (MFR) = 11, HDPE(11), MFR = 50, LLDPE(50)] as the sheath and general-purpose PET (IV = 0.65 dL/g) as the core through an annular spinneret using two different extrusion systems. Each system consisted of an extruder and a gear pump. The coaxially combined polymer melts were extruded through a single hole spinneret (0.5 mm diameter) at 290°C and at a total mass flow rate of 5 g/min. We maintained the mass flow rate combination at PE : PET = 1 : 1. The extruded fibers were wound by a winding device at 330 cm below the spinneret. The bicomponent fibers were produced at various take-up velocities of from 1 to 6 km/min. The schematic illustration of the spinning setup is presented in Figure 1.

Birefringence

We measured the birefringence of both the sheath and core in the bicomponent fiber using an interference microscope (Carl-Zeiss Jena) equipped with a polarizing filter. The method is described in the literature.[10,11] A typical interference fringe pattern of the bicomponent fiber observed under the interference microscope is shown in Figure 2. The refractive indices of the sheath and core parts, n_{out} and n_{in} are given below:

$$\frac{a_{out}}{A} \cdot \frac{\lambda}{2} = (n_{out} - N)(R_{out}^2 - R_{in}^2)^{1/2} \quad (1)$$

$$\frac{a_{in}}{A} \cdot \frac{\lambda}{2} = (n_{out} - N)(R_{out} - R_{in}) + (n_{in} - N)R_{in} \quad (2)$$

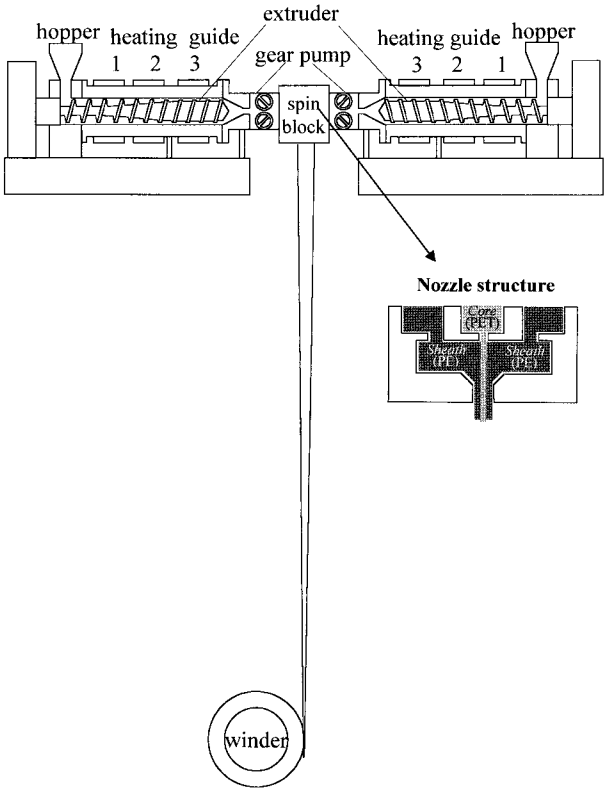

Figure 1 The setup used for melt spinning of a sheath/core bicomponent fiber.

where a_{out} and a_{in} are the fringe shifts measured at the interface between the sheath and core and at the center of the fiber, respectively; R_{out} and R_{in} are the outer and inner radii; N is the refractive index of the immersion liquid; and also λ is the wavelength of the incident light. Equation (2) allowed us to estimate the refractive index of the core component alone by subtracting the retardation effect of the sheath component covering the core component. We obtained the birefringence of the sheath and core as the difference between the corresponding refractive indices in parallel and perpendicular directions to the fiber axis.

Density

The density of the as-spun PE/PET bicomponent fibers was measured at 23°C using a density gradient method. The liquids used for the construction of the column were *n*-heptane and carbon tetrachloride.

Wide-Angle X-Ray Diffraction

Equatorial X-ray diffraction profiles were obtained by a Rigaku Denki X-ray diffractometer (D/max-III-A type) with an Ni-filtered Cu-Kα radiation source generated at 30 kV and −20 mA. The intensity distribution curves on the equator were also measured using a goniometer. The crystalline orientation was estimated by the azimuthal intensity distribution of well-resolved wide-angle X-ray reflection lines from the (200) and (020) planes. The crystalline orientations of the PET components were estimated by the azimuthal intensity distribution of well-resolved wide-angle X-ray reflection lines from the (100) and (010) planes, and the quantities of them were obtained by eq. (3).

$$f_c = \frac{180° - B°}{180°} \times 100 \tag{3}$$

where $B°$ is the half-width of the intensity distribution on the (100) and (010) planes on the equator of the PET component; and f_c has a value of 0 if the specimen is completely unoriented, and if the crystallites are all arranged perfectly parallel to one another it is equal to 100.

Dynamic Viscoelasticity

The dynamic viscoelasticity behavior was investigated using a Rheovibron DDV-II-C (Toyo Bald-

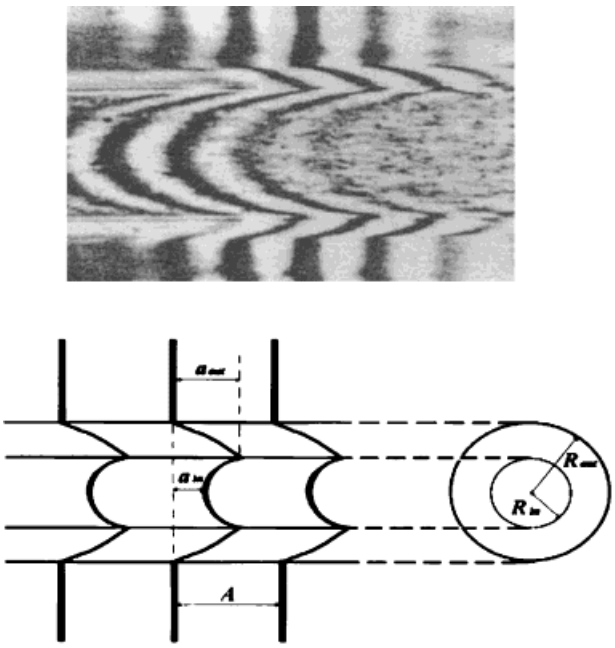

Figure 2 A typical micrograph and schematic illustration of the fringe pattern for the bicomponent fiber observed under an interference microscope.

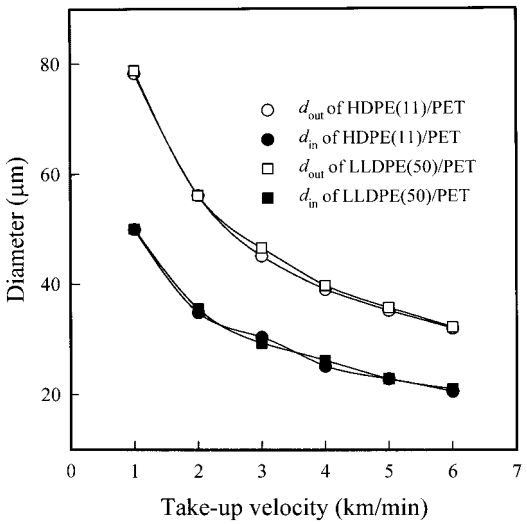

Figure 3 The diameter of PE/PET bicomponent fibers vs. the take-up velocity.

win) at a temperature range of 20–200°C with a heating rate of 2°C/min and a 110-Hz frequency.

Thermal Analysis

The thermal behaviors of PE/PET bicomponent fibers were investigated using differential scanning calorimetry (DSC, Shimazu DSC-50). It was measured with 5 mg of the fiber sample, which was cut into small pieces at a heating rate of 20°C/min up to 300°C.

Tensile Property

Tensile properties were measured using a Fafegraph-M tensile machine (Textechno) with a 10-mm length of monofilament at a crosshead speed of 20 mm/min. The initial Young's modulus, elongation at break, and tenacity were obtained by averaging at least 10 trials of the tensile test for each sample.

Interfacial Morphology

The interfacial morphology between the sheath and core and the existence of voids were confirmed by a polarized microscope (Zeiss). We observed the interfacial morphology and the voids under a polarized light by using the mixing refractive liquid with a refractive index similar to that of the PE component in the sheath.

RESULTS AND DISCUSSION

Diameter

Figure 3 shows the diameter of the PE/PET bicomponent fibers with the take-up velocity. With increasing take-up velocity the inner and outer radii both decreased gradually. The significant difference does not seem to exist between HDPE(11)/PET and LLDPE(50)/PET; the tendency may be because the spinline tension is almost all concentrated on the PET component.

Figure 4 shows changes of the core volume fraction with take-up velocities. The dotted lines represent the calculated core volume fraction in which the mass flow rate combination of the two components is 1 : 1. It is expected that the spinline is stable and independent of the take-up velocity and therefore the combination of the sheath and core components is arranged on a concentric circle.

Birefringence

Refractive indices parallel and perpendicular to the fiber axis, $n_{\parallel}$ and $n_{\perp}$, were measured by using an interference microscope. The PE components in the HDPE(11)/PET and LLDPE(50)/PET as-spun bicomponent fibers and the PE in the single-component as-spun fibers were plotted against the take-up velocity for comparison in Figure 5. The birefringences of the former are much lower in the overall take-up velocities than those of PE single-component fibers.[12,13] The birefringence of the PE component will be affected by the orientation-induced crystallization of PET. The birefringence of the HDPE(11) component of the bicomponent fiber slightly increased up to a take-up velocity of 3 km/min and then decreased. The

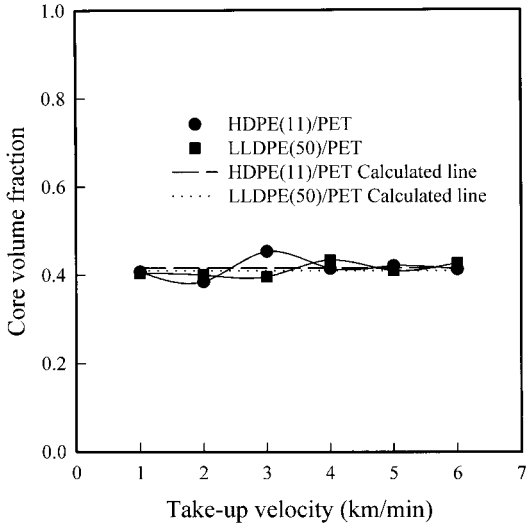

Figure 4 The core volume fraction of PE/PET bicomponent fibers vs. the take-up velocity.

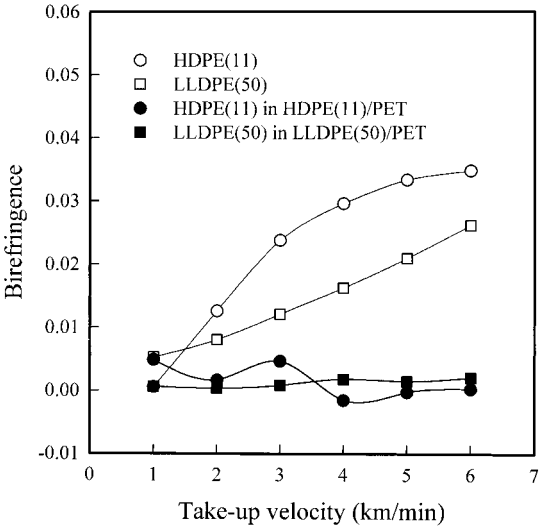

Figure 5 The change of birefringence with take-up velocity for the PE component in PE/PET bicomponent fibers. Birefringences for single-component fibers are also shown for comparison.

decrease in the range of take-up velocity of 3–4 km/min corresponds with the ranges of the early stage of orientation-induced crystallization in the PET component.[11] However, above the take-up velocity of 4 km/min the birefringence of the PE component seemed to be close to zero, indicating that the orientation of the PE component was remarkably suppressed.

Figure 6 shows the birefringences of PET components in the HDPE(11)/PET and LLDPE(50)/PET bicomponent fiber and that of a PET single-component fiber for comparison.[11] With increasing take-up velocity, the molecular orientation of PET is supposed to be promoted and hence the birefringence increases remarkably. Above 3 km/min, the birefringence of the PET component in LLDPE(50)/PET became slightly larger than that of the PET component of HDPE(11)/PET. The molecular orientation of the PET component, which experiences higher elongational stress in the spinline, is promoted with increasing take-up velocity, thereby leading to the increase in birefringence.

Lorentz–Lorenz Density and (Mass) Density

The Lorentz–Lorenz equation expresses the relation between the refractive index (n) and the density (ρ) of the filament as follows:

$$\frac{\bar{n}^2 - 1}{\bar{n}^2 + 2} = \frac{4\pi N\rho}{3M} P \tag{4}$$

where N, M, and P denote the Avogadro number, the molecular weight, and the molar polarizability, respectively. For a uniaxially anisotropic material such as filaments, the mean refractive index $\bar{n}$ may be expressed using the refractive indices parallel ($n_{\parallel}$) and perpendicular to the principal ($n_{\perp}$) axis as follows:

$$\bar{n}^2 = \frac{2n_{\perp}^2 + n_{\parallel}^2}{3} \tag{5}$$

According to eqs. (3) and (4), the term $(\bar{n}^2 - 1)/(\bar{n}^2 + 2)$ is directly proportional to the density. Hereafter we call this the Lorentz–Lorenz density.

Figure 7 shows Lorentz–Lorenz densities of the PE component in HDPE(11)/PET and LLDPE(50)/PET bicomponent fibers and PE single-component fibers with take-up velocities for comparison. The tendency in the Lorentz–Lorenz densities of the PE component in HDPE(11)/PET and LLDPE(50)/PET bicomponent fibers is similar to that of HDPE and LLDPE for single-component fibers. The reason for this is that the fraction of the crystalline and amorphous region is nearly unaffected by the increasing take-up velocity because of the rapid crystallization of the PE component. On the other hand, the difference in the optical density of the PE components between the HDPE(11)/PET and LLDPE(50)/PET bicompo-

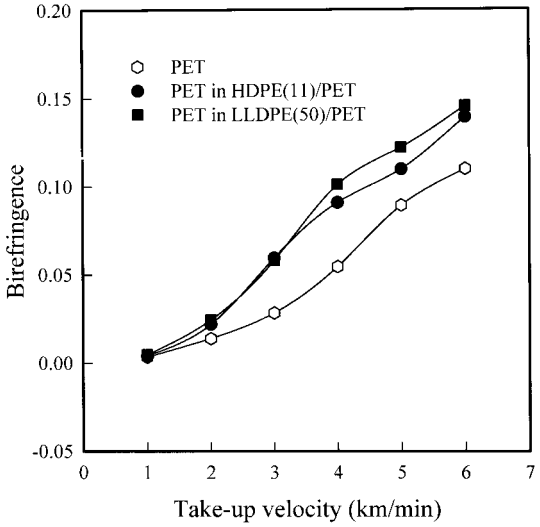

Figure 6 The change of birefringence with take-up velocity for the PET component in PE/PET bicomponent fibers. Birefringences for single-component fibers are also shown for comparison.

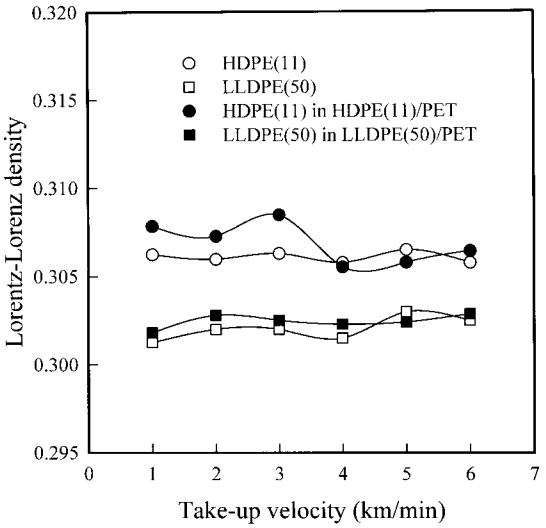

Figure 7 The relation between the Lorentz–Lorenz density and take-up velocity for the PE component in PE/PET bicomponent fibers. Lorentz–Lorenz densities for a single-component fiber are shown for comparison.

nent fibers may be ascribed to the difference in the respective intrinsic densities.

Figure 8 shows the Lorentz–Lorenz densities of the PET component with take-up velocities, which are calculated from the refractive indices of the PET component in PE/PET bicomponent fibers. Up to a take-up velocity of 3 km/min, the Lorentz–Lorenz densities are little changed. But

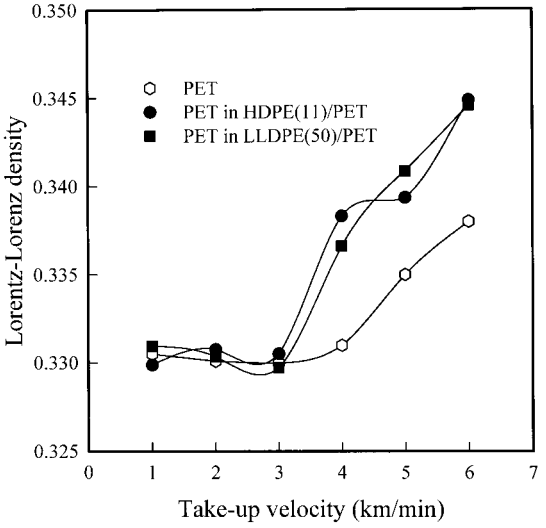

Figure 8 The relation between Lorentz–Lorenz density and take-up velocity for the PET component in PE/PET bicomponent fibers. Lorentz–Lorenz densities for a single-component fiber are also shown for comparison.

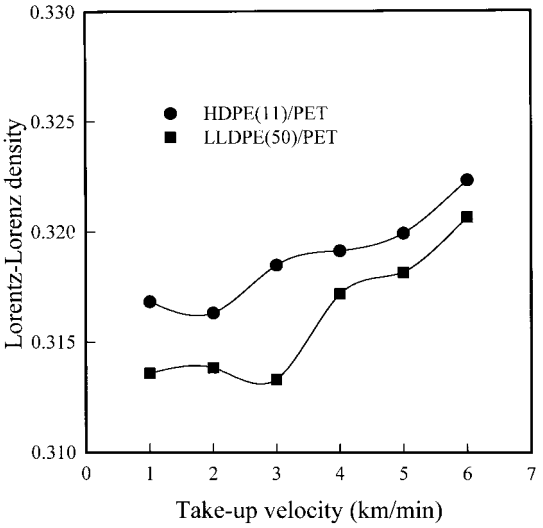

Figure 9 The estimated Lorentz–Lorenz density of PE/PET bicomponent fibers vs. the take-up velocity.

above a take-up velocity of 4 km/min, the increase of Lorentz–Lorenz density is corresponding to the onset of the orientation-induced crystallization; this increase is remarkable in comparison with the PET single-component fiber.

Figure 9 shows Lorentz–Lorenz densities of PE/PET bicomponent fibers with take-up velocities, which are calculated from the rule of mixture by the volume fraction of the PET component in the core. With increasing take-up velocity, the packing between the molecular chains is improved because of the increase of the orientation.

Figure 10 shows the changes of the mass density of HDPE(11)/PET and LLDPE(50)/PET bicomponent fibers with take-up velocities. The solid lines represent the characterized densities in the density gradient column. With increasing take-up velocity the density is gradually increased. It is supposed that the density of a PE single-component fiber changes little with the overall take-up velocities and that of a PET single-component fiber is wholly increased because of the orientation-induced crystallization.[11–13] Also, the density of the PE/PET bicomponent fiber increases slightly with increasing take-up velocity. The dotted lines in Figure 10 represent the density calculated from the rule of mixture using the respective densities of HDPE(11), LLDPE(50), and PET spun as a single filament. There is a little difference between the solid and dotted line. We guess that the increment of the density is due to the orientation-induced crystallization of the PET component in the PE/PET bicomponent fiber.

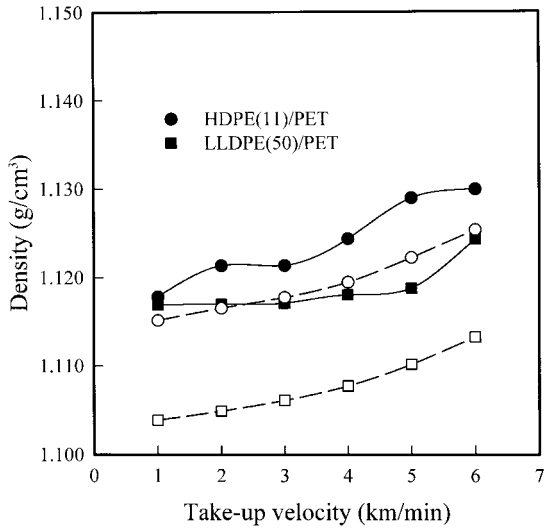

Figure 10 The density of HDPE(11)/PET and LLDPE(50)/PET bicomponent fibers vs. the take-up velocity. (—) The measured density by the density gradient method, and (- - -) the calculated density using the rule of mixture.

Figure 11 shows the correlations between the experimental (mass) density in Figure 10 and the Lorentz–Lorenz density calculated from the rule of mixture using the conjugated volume fraction. This shows a good correlation; accordingly, the packing of the molecular chains for the respective components in the bicomponent fiber can be estimated.

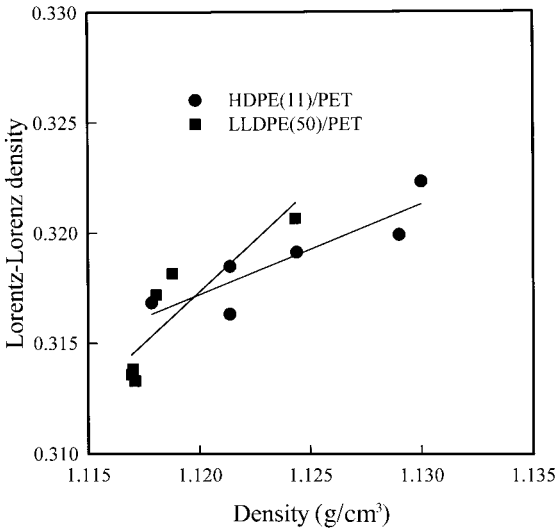

Figure 11 The relation between the mass density and Lorentz–Lorenz density for HDPE(11)/PET and LLDPE(50)/PET bicomponent fibers.

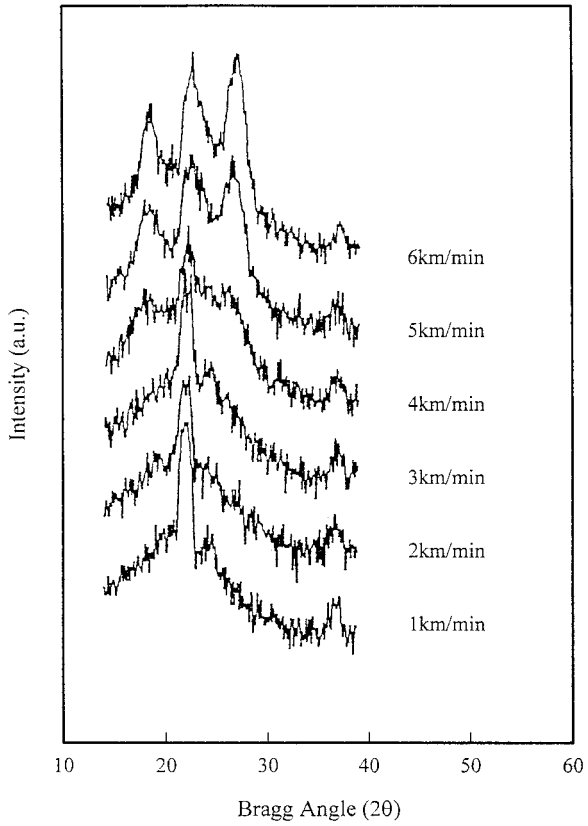

Figure 12 Wide-angle X-ray equatorial scans of HDPE(11)/PET bicomponent fibers vs. the take-up velocity.

Crystalline Structure

Equatorial X-ray diffraction profiles of high-speed spun HDPE(11)/PET and LLDPE(50)/PET bicomponent fibers are shown in Figures 12 and 13, respectively. With increasing take-up velocity, the intensities of the diffraction peak for two PE/PET bicomponent fibers increase. Up to 3 km/min, the reflections from the (110) plane near $2\theta = 22$, the (200) plane near $2\theta = 24.27$, and the (020) plane near $2\theta = 36.8$ were observed for the PE component. These phenomena are due to the rapid crystallization of PE rather than the effect of orientation-induced crystallization with take-up velocities for the PET component. At the take-up velocity of 4 km/min, the reflections from the (100) plane near $2\theta = 26.4$ and from the (010) plane near $2\theta = 17.85$ are observed for the PET component. With increasing take-up velocity the peaks are remarkably sharpened, suggesting that the orientation-induced crystallization of the PET components has progressed. These phenomena correspond with the results of both the birefrin-

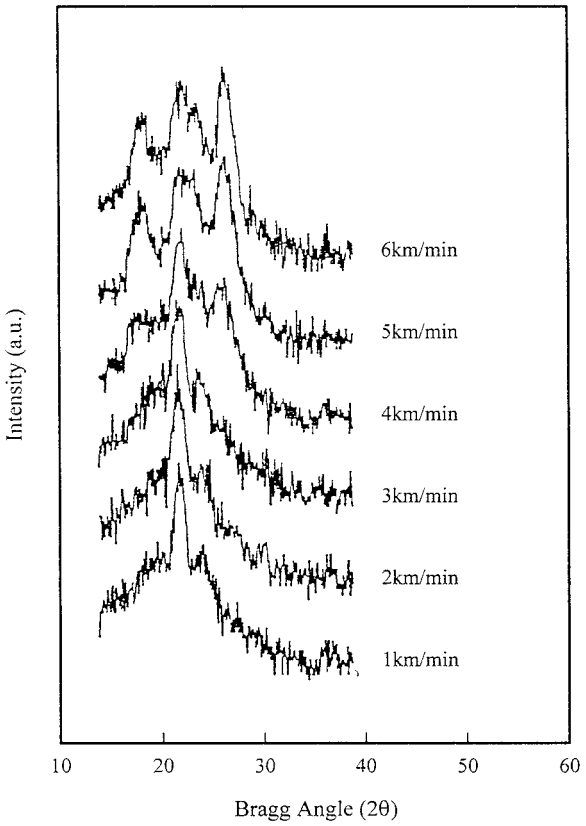

Figure 13 Wide-angle X-ray equatorial scans of LLDPE(50)/PET bicomponent fibers vs. the take-up velocity.

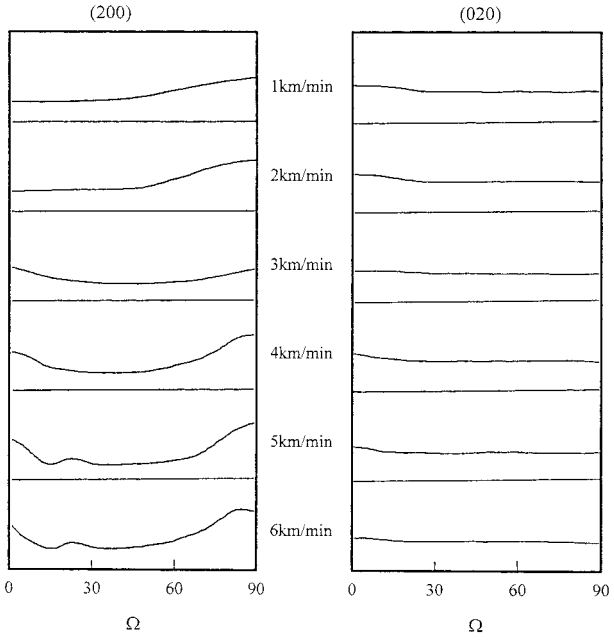

Figure 14 The azimuthal variation of (200) and (020) intensities according to the take-up velocity for the PE component in HDPE(11)/PET bicomponent fibers.

gence (Fig. 6) and Lorentz–Lorenz density calculated from birefringence (Fig. 8), which are suddenly increased at the take-up velocity of 4 km/min.

Crystalline Orientation

Figure 14 shows the azimuthal diffraction curves of the (200) and (020) reflections of the HDPE component in the HDPE(11)/PET bicomponent fiber at various take-up velocities. The (200) plane of crystals for the HDPE component is oriented to the a-axis direction up to a take-up velocity of 2 km/min, and it is oriented to mixed loading of the a-axis and c-axis orientation above a take-up velocity of 3 km/min. This tendency can be explained by considering the fact that the spinline tension is mainly concentrated in the PET component and the tension affects a little in the PE, and then the distribution of the a-axis and c-axis orientation occurs.

Figure 15 shows azimuthal diffraction curves of (200) and (020) reflections of the LLDPE component in LLDPE(50)/PET bicomponent fiber with take-up velocities. In a range of take-up velocity of 1–2 km/min the orientation of PE closes

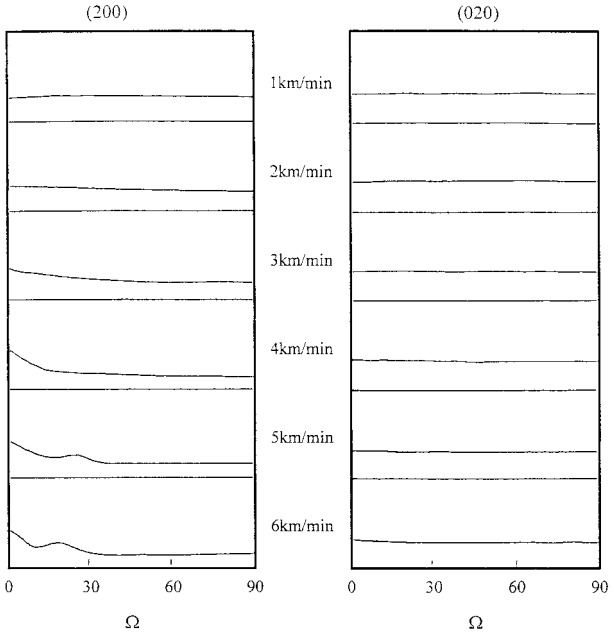

Figure 15 The azimuthal variation of (200) and (020) intensities according to the take-up velocity for the PE component in LLDPE(50)/PET bicomponent fibers.

Table I Relation between Take-Up Velocity and Crystalline Orientation Factor of PET Component for Two Bicomponent Fibers

	Take-Up Velocity		
Sample	4 km/min	5 km/min	6 km/min
PET	0.746	0.895	0.910
HDPE(11)/PET	0.865	0.916	0.923
LLDPE(50)/PET	0.898	0.920	0.924

to nearly nonorientation, and afterward the orientation of the (200) plane is confirmed; then the orientation of the a axis is only improved with increasing take-up velocity as in the HDPE(11)/PET bicomponent fiber. We suppose that the orientation is prone to propagate because of little extensional viscosity on the spinline. These results correspond with the birefringence of the PE component in Figure 5.

Table I shows the crystalline orientation factor of PET components obtained from the azimuthal scans of (100) and (010) planes in HDPE(11)/PET and LLDPE(50)/PET bicomponent fibers. In the crystalline orientation factors of the PET component in bicomponent fibers compared with PET single-component fibers the effects on the increment of take-up velocity are more rapid. We confirmed it as promoting the crystalline orientation of the PET component by conjugating it with HDPE and LLDPE.

Dynamic Viscoelasticity

Figure 16 shows the plots of tan δ versus temperature for HDPE(11)/PET bicomponent fibers at various take-up velocities. Because the thermal stability of the HDPE(11) component in the sheath is relatively low, the curves have a discontinuity (arrow in Fig. 16) near the melting temperature of HDPE(11). Hence, the tan δ peaks of the PET component shift to the lower temperature, and the intensities of the tan δ peak decrease. This tendency means that the packing density of the amorphous region in PET is relatively low with increasing take-up velocity and the volume of the amorphous region decreases. Accordingly, it is considered to correspond to the typical tan δ behavior in the PET single-component fiber on high-speed spinning.[11,14] The shoulder based on the crystalline relaxation of HDPE is shown near 90°C, and the obvious peak near 130°C is due to the amorphous dispersion of PET.

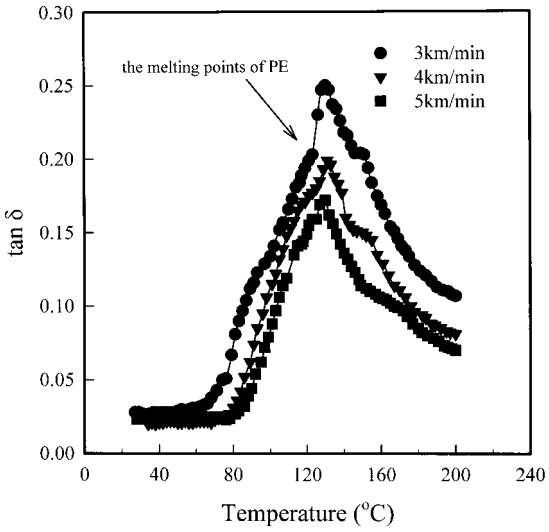

Figure 16 The tan δ vs. temperature for the HDPE(11)/PET as-spun bicomponent fiber at various take-up velocities at 110 Hz.

Figure 17 shows the tan δ curves of LLDPE(50)/PET bicomponent fiber; the tendency is similar to that of HDPE(11)/PET.

Thermal Behavior

In the melt-spinning process of PET fiber with increasing take-up velocity, the molecular orientation in spun yarn generally increases before the solidification and crystallization temperature ($T_{c\text{-cold}}$) is shifted lower. These tendencies have lin-

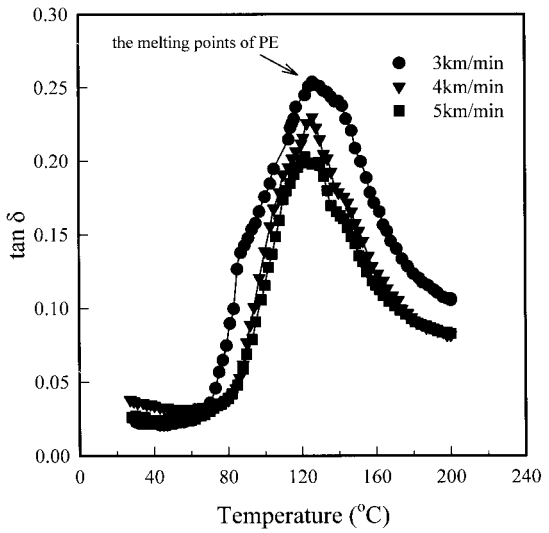

Figure 17 The tan δ vs. temperature for the LLDPE(50)/PET as-spun bicomponent fiber at various take-up velocities at 110 Hz.

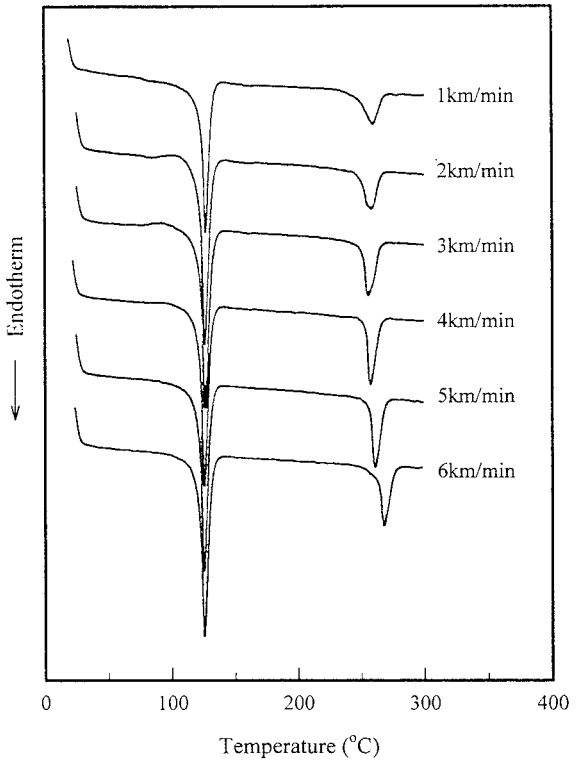

Figure 18 DSC thermograms for HDPE(11)/PET bicomponent fibers obtained at various take-up velocities.

ear correlations with the increase of molecular orientation.[15] Therefore, the correlationship between the orientation factor (same as birefringence) and the temperature of the $T_{c\ \mathrm{cold}}$ peak is used as a guidepost for the orientation.

A DSC thermogram of HDPE(11)/PET bicomponent fibers is shown in Figure 18. The $T_{c\ \mathrm{cold}}$ of PET is hardly invisible, because the $T_{c\ \mathrm{cold}}$ of PET and melting temperature (T_m) of HDPE are almost the same. In the take-up velocities of 1–3 km/min, the $T_{c\ \mathrm{cold}}$ peaks of PET are observed. The $T_{c\ \mathrm{cold}}$ of PET in PET single-component fiber is obviously observed up to a take-up velocity of 3 km/min.[11] But the $T_{c\ \mathrm{cold}}$ of PET in HDPE(11)/PET bicomponent fiber is plainly observed up to a take-up velocity of 3 km/min because of the increase of orientation by the orientation-induced crystallization. With increasing take-up velocity the endothermic peaks related to the melting temperature of the HDPE component are uniform. Up to a take-up velocity of 3 km/min, the $T_{c\ \mathrm{cold}}$ peak of the PET component becomes low because of the high orientation of the PET molecules, but above a take-up velocity of 4 km/min the $T_{c\ \mathrm{cold}}$ peaks disappear because of the orientation-induced crystallization of the PET component in the spinning process. Accordingly, the melting temperature increases above a take-up velocity of 4 km/min.

A DSC thermogram of LLDPE(50)/PET bicomponent fibers is shown in Figure 19. The figure shows that in the take-up velocity of 1–2 km/min the $T_{c\ \mathrm{cold}}$ of the PET component is observed more clearly compared to HDPE(11)/PET bicomponent fibers at temperatures just above the T_m of LLDPE, while at a take-up velocity 3 km/min it appears at a temperature just below the T_m of LLDPE and finally disappears above a take-up velocity 4 km/min. It is known that the orientation-induced crystallization of the PET component in LLDPE(50)/PET bicomponent fiber occurs more rapidly than in the PET single-component fiber like the results of the birefringence and so forth.

Tensile Property

Figures 20 and 21 show the stress–strain curves of HDPE(11)/PET and LLDPE(50)/PET bicomponent fibers with take-up velocities, respectively.

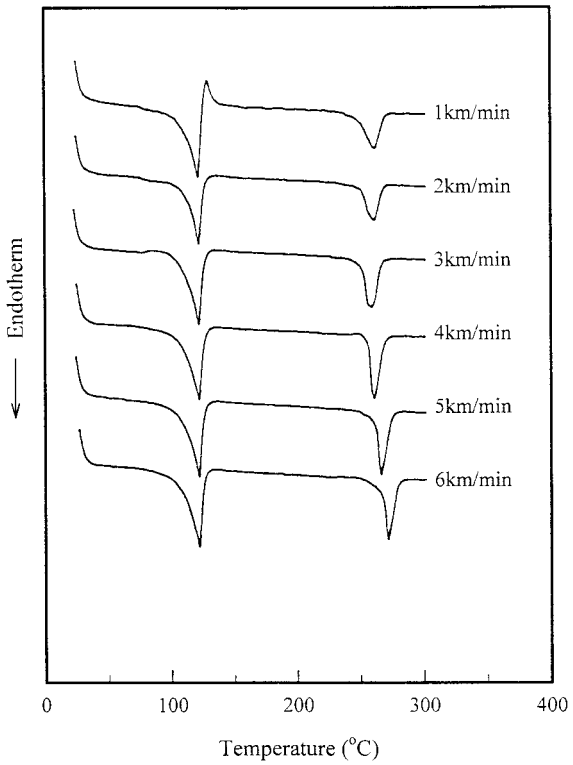

Figure 19 DSC thermograms for LLDPE(50)/PET bicomponent fibers obtained at various take-up velocities.

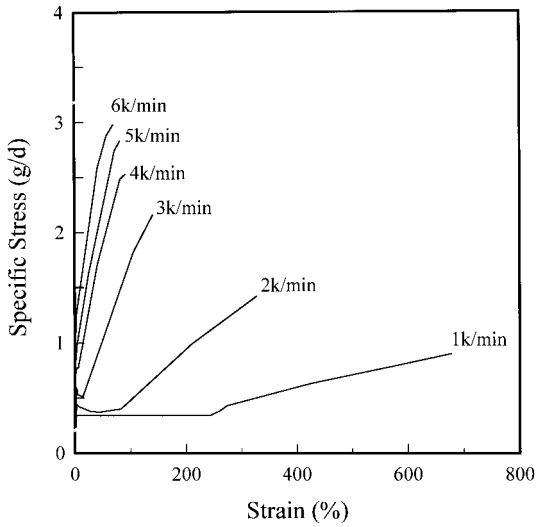

Figure 20 Stress–strain curves of HDPE(11)/PET bicomponent fibers obtained at various take-up velocities.

The initial modulus, specific stress, strain, and work of rupture are shown in Table II with increasing take-up velocity; the strain decreases and the stress and initial modulus increase. Above a take-up velocity of 3 km/min, the orientation-induced crystallization of the PET component occurs and the mechanical property is sharply increased. This corresponds with the results of birefringence in Figure 6. Compared with the PET single-component fiber,[11] the physical properties of the HDPE(11)/PET and LLDPE(50)/PET bicomponent fibers are better, because the fiber structure formations are promoted for coextrusion and PE has the lower viscosity.

The physical properties of HDPE(11)/PET and LLDPE(50)/PET bicomponent fibers were found to be comparable to each other with increasing take-up velocity. In particular, the physical properties of PE/PET bicomponent fibers are not affected by the differences of types and MFR on the PE component. Accordingly, the physical properties of bicomponent fiber proved to mainly depend on the PET component, which undergoes enhanced structural development by a conjugation with the PE component.

Interfacial Morphology

Figure 22 shows the pattern obtained from a polarized microscope in the refractive liquid, which is similar to the refractive index of HDPE(11). We can observe the morphology of the core because the refractive index of the immersing liquid is similar to the refractive index of the sheath component. It is possible that the expansion coefficients of HDPE(11) and PET are different from each other. Although the instability of the interface is caused by excessive spinline tension in high-speed spinning, the HDPE(11) and PET are arranged on a concentric circle. The void and instability in the interface are shown above a take-up velocity of 4 km/min, where the orientation-induced crystallization of PET starts.

Figure 23 shows the changes of the interfacial morphology for LLDPE(50)/PET bicomponent fibers obtained at various take-up velocities. Han et al.[16–18] reported that the shapeable stability in sheath/core bicomponent fiber is prone to increase the differences between the sheath and core component viscosity and first normal stress. Consequently, it is supposed that LLDPE(50)/PET has a larger difference in viscosity and a higher stability in the interface compared to the HDPE(11)/PET bicomponent fibers. It is confirmed that the separation of the interface and the instability occurs above 4 km/min in LLDPE(50)/PET. Accordingly, the difference between the density characterized from the density gradient method and the density calculated by the rule of mixture is not clearly observed at high take-up velocities.

If the cross section of a fiber is circle shaped, the diameter is calculated from eq. (6):

$$d = 11.89416 \times \sqrt{\frac{D}{\rho}} \tag{6}$$

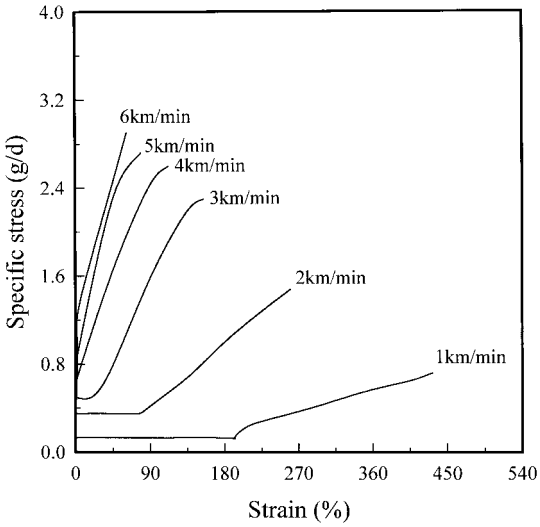

Figure 21 Stress–strain curves of LLDPE(50)/PET bicomponent fibers obtained at various take-up velocities.

Table II Mechanical Properties of HDPE(11)/PET and LLDPE(50)/PET Bicomponent Fibers in High-Speed Spinning

Take-Up Velocity (km/min)	Initial Modulus (g/d)		Specific Stress (g/d)		Strain (%)		Work of Rupture (g × cm)	
	HDPE(11)/PET	LLDPE(50)/PET	HDPE(11)/PET	LLDPE(50)/PET	HDPE(11)/PET	LLDPE(50)/PET	HDPE(11)/PET	LLDPE(50)/PET
1	11.61	11.95	0.92	0.72	638.10	440.72	171.32	147.05
2	13.26	13.37	1.43	1.46	329.06	261.12	62.39	88.49
3	24.43	20.93	2.16	2.31	141.42	147.01	53.73	56.79
4	35.00	31.83	2.55	2.58	92.59	110.63	35.73	42.30
5	42.88	40.66	2.84	2.82	83.49	80.08	31.29	29.79
6	50.22	48.91	2.97	2.95	68.55	61.85	24.23	22.51

where the diameter (d) of the fiber with free void is obtained using the density (ρ) and the fineness (D) of the fiber. To estimate the instability of the interface, the diameter characterized from the microscope and the diameter calculated from eq. (6) are both plotted in Figure 24.

It is known that there is very little difference between the diameter characterized with the microscope and the diameter calculated from eq. (6). In spite of the interfacial instability increasing with the take-up velocity, as in Figure 22, it was confirmed that the density of the two polymer can be characterized through the density gradient liquid.

CONCLUSION

High-speed spinning of HDPE(11)/PET and LLDPE(50)/PET bicomponent fibers was carried out,

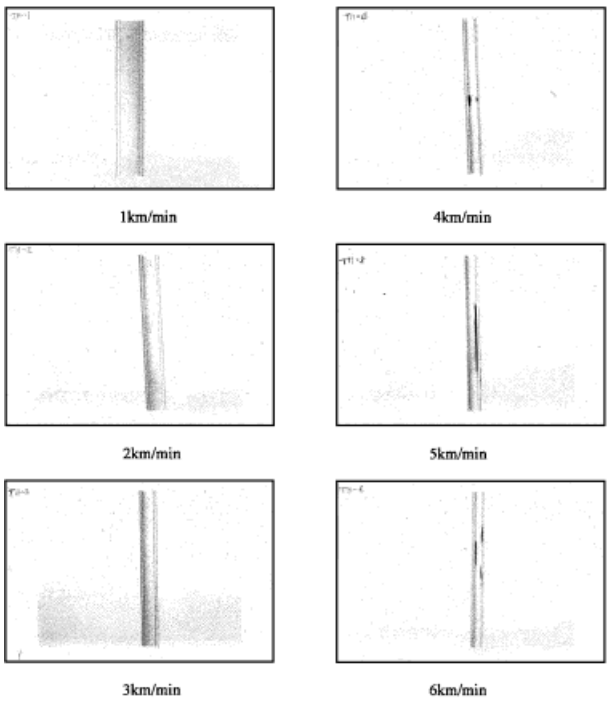

Figure 22 The changes in the interfacial morphology for HDPE(11)/PET bicomponent fibers obtained at various take-up velocities.

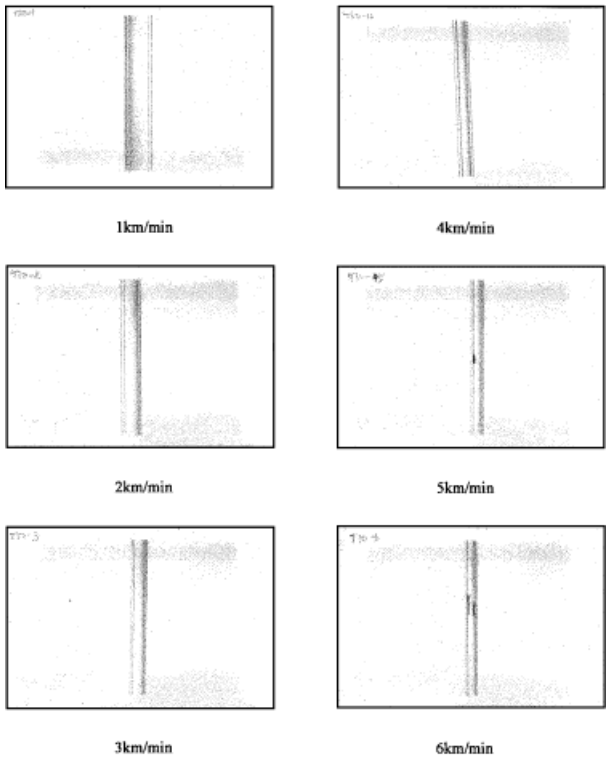

Figure 23 The changes in the interfacial morphology for LLDPE(50)/PET bicomponent fibers obtained at various take-up velocities.

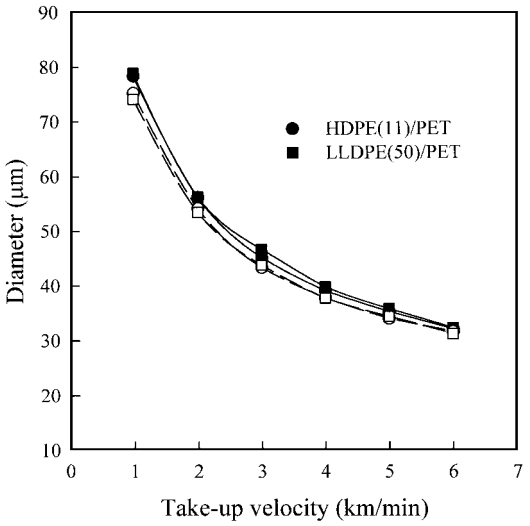

Figure 24 The diameter of PE/PET bicomponent fibers vs. the take-up velocity. (—) The diameter measured by a polarized microscope, and (- - -) the calculated diameter using eq. (5).

and the fiber structure formation and physical properties on take-up velocities were investigated with birefringence, wide-angle X-ray diffraction, thermal analysis, tensile tests, and so forth.

1. In the fiber structure formation of PE/PET, the PET component was developed but the PE components were suppressed in high-speed spinning.
2. The different kinds of PE had little affect on the fine structure formation of the bicomponent fiber.
3. The difference in the mechanical properties of bicomponent fiber with the MFR was very little.
4. An interface instability was shown above a take-up velocity of 4 km/min, where the orientation-induced crystallization of PET started. LLDPE(50)/PET had the larger difference in intrinsic viscosity and a higher stability in the interface compared to the HDPE(11)/PET bicomponent fibers.

REFERENCES

1. Nakajima, T. Advanced Fiber Spinning Technology; Woodhead Publishing Ltd.: Cambridge, U.K., 1994.
2. Stibal, W.; Schach, G. Chem Fiber Int 1995, 45, 296.
3. Tomioka, S.; Kojima, M. Sen'i Gakkaishi 1980, 36, T201.
4. Tomioka, S.; Kojima, M. Sen'i Gakkaishi 1979, 35, T542.
5. Cho, H. H.; Kikitani, T. J Kor Fiber Soc 1996, 33, 360.
6. Radhakrishnan, J.; Kikutani, T.; Okui, N. Sen'i Gakkaishi 1996, 52, 618.
7. Radhakrishnan, J.; Kikutani, T.; Okui, N. Text Res J 1997, 67, 684.
8. Kikutani, T.; Radhakrishnan, J.; Arikawa, S.; Takaku, A.; Okui, N.; Jin, X.; Niwa, F.; Kudo, Y. J Appl Polym Sci 1996, 62, 1913.
9. Kikutani, T.; Arikawa, S.; Takaku, A.; Okui, N. Sen'i Gakkaishi 1995, 51, 408.
10. Shimizue, J.; Okui, N.; Kikutani, T. Sen'i Gakkaishi 1981, 37, T135.
11. Park, J. B.; Kim, K. H.; Bang, Y. H.; Cho, H. H. J Kor Fiber Soc 1996, 33, 798.
12. Cho, H. H.; Kim, K. H.; Ito, H.; Kikutani, T. J Appl Polym Sci, to appear.
13. Cho, H. H.; Kim, K. H.; Ito, H.; Kikutani, T. J Appl Polym Sci, to appear.
14. Kamid, K.; Kuriki, T. J Text Machinery Soc Jpn 1985, 38, 268.
15. Turi, E. A. Thermal Characterization of Polymeric Materials; Academic: New York, 1983; Chap. 7.
16. Han, C. D.; Lamonte, R. R. J Polym Eng Sci 1972, 11, 385.
17. Han, C. D.; Lamonte, R. R. J Appl Polym Sci 1973, 17, 1165.
18. Han, C. D.; Kim, Y. W. J Appl Polym Sci 1974, 18, 2589.